HYDROGEN DIFFUSION AND TRAPPING IN 42CrMo4 QUENCHED AND TEMPERED STEEL: INFLUENCE OF QUENCHING TEMPERATURE AND PLASTIC DEFORMATION

A. Zafra*, J. Belzunce, and C. Rodríguez
University of Oviedo, campus universitario, east building, 33203, Gijón, Spain
*Corresponding author: Alfredo Zafra García (+34 985182023) zafraalfredo@uniovi.es

ABSTRACT

Medium- and high-strength steel components working in contact with hydrogen-rich environments must be appropriately designed in order to provide safe and reliable service during their entire lifespan. In this context, the present paper aims to study hydrogen diffusion and trapping in a quenched and tempered 42CrMo4 steel by means of electrochemical permeation methods. The effect of quenching from a high austenitizing temperature and applying a plastic deformation of 10% and 20%, were also evaluated.

In general terms, the results showed that with increasing cathodic current (amount of hydrogen introduced in the steel specimen), the apparent hydrogen diffusion coefficient also increases up to a maximum constant value that corresponds to the lattice hydrogen diffusion coefficient, D_L. Quenching the steel from a high austenitizing temperature decreases hydrogen diffusivity and increases the density of traps. On the other hand, microstructural trapping increases (increase in the dislocation density) and the diffusion coefficients decrease after applying a cold plastic deformation. All the aforementioned modifications related to the permeation of hydrogen throughout the microstructure of the steel were finally correlated with changes in the steel´s hardness.

KEYWORDS: Hydrogen permeation, hydrogen diffusion, materials degradation, hydrogen trapping, 42CrMo4 steel.

1. INTRODUCTION

Hydrogen atoms can enter into steel components during pickling, electric discharge machining, electrolytic coating from aqueous media, cathodic protection and also due to corrosion phenomena in different environments [1-4]. Under these circumstances, proton reduction results in the formation of adsorbed hydrogen atoms on the steel surface and, although most of the adsorbed hydrogen atoms evolved from the steel surface as hydrogen molecules (two adsorbed hydrogen atoms combine to form a hydrogen H_2 molecule), part of them are absorbed into the steel as atomic hydrogen. The hydrogen absorbed by structural steels can produce significant embrittlement, characterized by a drastic reduction in their most important mechanical properties (tensile strength, elongation, fracture toughness and fatigue crack propagation rate) [5-8]. Therefore, the characterization of hydrogen behaviour in steels is important for the understanding, prediction, and prevention of hydrogen embrittlement.

Internal hydrogen is present in steels either as interstitial atoms located in interstitial lattice sites or trapped at specific microstructural locations, such as dislocations, grain boundaries, internal interphases, non-metallic inclusions, etc. [9]. In this latter case, a distinction is usually made between reversible and irreversible trapping based on the binding energy of each trap. Traps with a high binding energy (>50 kJ/mol) are defined as irreversible traps and the hydrogen atoms trapped in them are considered non-diffusible. Reversible traps, on the other hand, are sites from which hydrogen atoms can escape due to fluctuations in thermal energy. The diffusible hydrogen, i.e. the hydrogen able to move through the steel microstructure, is hence the sum of interstitial and reversible hydrogen atoms, and local equilibrium is usually assumed to exist between the two [10, 11]. Reliable and useful information on all these processes

can be obtained using electrochemical permeation techniques, locating the specimen of interest between hydrogen charging and oxidation electrolytic cells. Furthermore, thermal desorption analysis (TDA), usually used to determine hydrogen desorption characteristics, provides useful and complementary information about trapping sites and hydrogen contents.

The evaluation of hydrogen uptake, permeation and transport in metals using electrochemical techniques was developed by Devanathan and Stachurski [12]. Both the practical use and guidelines of these techniques regarding the preparation of specimens, control and monitoring of environmental variables, test procedure and analyses of results are described in the ASTM G148 standard [13]. In these tests, a thin metal membrane (the working specimen) is placed for testing between two independent electrochemical cells. Hydrogen is then introduced into the membrane entry side and diffuses through the membrane until escaping through its exit side, where it is immediately electrochemically oxidised and detected as a density current.

The practical use of permeation tests is based on the existence of well-defined hydrogen entry conditions on the input side of the membrane (rapid establishment of a certain hydrogen concentration beneath the entry side of the tested specimen) in order to ensure that the measured permeation hydrogen flux is fully controlled by diffusion laws and that hydrogen transport is mainly due to hydrogen atoms hopping between interstitial lattice sites. However, the facts that surface processes on the entry side are usually quite slow and that hydrogen trapping or de-trapping always takes place during hydrogen transport through the membrane specimen may also be considered. These problems especially affect structural steels, in which the mobility of hydrogen is high, and which also have a high trapping capacity [14]. The use of successive partial build-up and decay transients produced by a relatively small increase or decrease in hydrogen concentration has been proven to be a good technique to reduce these problems [14, 15].

Assuming that the kinetics of hydrogen transport is governed by diffusion through the lattice (interstitial diffusion), along with trapping and de-trapping at specific microstructural sites, permeation results hence are dependent on the progressive filling of both reversible and irreversible traps. Therefore, hydrogen diffusivity is sensitive to the increase in the subsurface hydrogen concentration, increasing with it until a constant value is detected. That value corresponds to the real lattice hydrogen diffusion coefficient of the steel, when all the microstructural traps have been completely filled [16-18].

Typically, single hydrogen permeation tests are performed by applying a constant cathodic current density until the permeation current density reaches a steady state value, J_{ss}. The most common values of this current found in the literature vary between 1 and 10 mA/cm^2, although smaller or larger cathodic current density values have sometimes been applied. For example [19] used 0.25 mA/cm^2, whereas, [17] applied cathodic currents within the range of 5-200 mA/cm^2. In tests of this type, a unique value of the hydrogen diffusion coefficient, D_{app}, is calculated. This permeation transient is usually followed by a decay transient (hydrogen discharge phase), during which hydrogen effuses out of the specimen after the cathodic current is switched off. This procedure is often used to determine the density of reversible traps in the steel. Nevertheless, depending on the steel microstructure (traps nature and density) and the applied cathodic current (amount of hydrogen generated on the hydrogen charged surface of the specimen), the single permeation transient methodology is not appropriate to fully characterize the interaction between hydrogen and microstructure, as microstructural traps are progressively filled and the hydrogen diffusion coefficient is not constant but in fact dependent on trap filling. In this respect, hydrogen permeation standard ASTM G148 [13] advises performing at least two consecutive processes of hydrogen charge and discharge in order to measure hydrogen diffusion in the presence of empty and filled microstructural traps. In fact, [20] performed three successive hydrogen charge/discharge cycles in order to characterize diffusivity in a structural steel with different pre-strains. Additionally, [21,22] have demonstrated the need to record successive permeation transients in order to study the evolution of the hydrogen diffusion coefficient versus the applied cathodic current. Moreover, the partial charge/discharge method proposed by Zakroczymski [23] and extensively applied by [24-27] has proven to be a convenient technique to measure diffusion coefficients under equilibrium conditions and thus determine diffusion coefficients.

As previously mentioned, the transport of hydrogen in steels is affected by numerous factors. In particular, plastic deformation and internal stresses can lead to a notable change in hydrogen mobility and trapping. Kumnick and Johnson [28] investigated the effect of cold plastic deformation on hydrogen diffusion in annealed Armco steel, while other authors have performed similar studies in different irons and steels [20, 29-31]. All these researchers observed a delay in hydrogen diffusivity when increasing the applied plastic deformation, as the greater the applied strain, the greater the dislocation density in the steel, which comprises the most important source of microstructural traps in conventional steels. The binding energy generally attributed to dislocations is around 25-30 kJ/mol [9, 32-35]. The increase in dislocation density due to plastic deformation will hence increase the amount of reversible hydrogen trapped in the steel, thereby increasing hydrogen embrittlement. On the other hand, [36] reports that hydrogen diffusion coefficient decreases and hydrogen absorption increases with the increase of the austenitizing temperature, and similar results were obtained by [37] when coarser grain sizes were produced applying a higher heat input in welding.

In this study, we have combined electrochemical permeation tests and thermal desorption analysis to identify hydrogen diffusion and trapping phenomena in a quenched and tempered 42CrMo4 steel. The effects of quenching from a high austenitizing temperature in order to increase the prior austenite grain size and the application of a cold plastic deformation were also studied.

2. EXPERIMENTAL PROCEDURE

2.1 Material

A commercial 42CrMo4 steel was used in the present study. Its chemical composition is shown in Table 1.

Table 1. Chemical composition of 42CrMo4 steel (weight %)

Steel	C	Cr	Mo	Mn	Si	P	S
42CrMo4	0.42	0.98	0.22	0.62	0.18	0.008	0.002

Hot rolled plates (250x250x12 mm^3) of 42CrMo4 steel (normalized and tempered) were submitted to a heat treatment consisting in austenitizing at 845ºC for 40 min, followed by quenching in room temperature water (WQ) and tempering at 700ºC for 2 h (42CrMo4_700).

The room temperature (RT) hardness, tensile properties, and fracture toughness of the steel, obtained in previous studies [38,39], are summarized in Table 2.

Table 2. Hardness (HV), tensile properties and fracture toughness of 42CrMo4_700 steel grade [38, 39]

Steel Grade	Heat treatment	HV	σ_{ys} [MPa]	σ_{uts} [MPa]	E [%]	RA [%]	$J_{0.2/BL}$ [kJ/m^2]
42CrMo4_700	845ºC/40min+WQ+T700ºC/2h	207	622	710	22	61	580

Different degrees of plastic deformation were applied at RT in a laboratory rolling mill in order to correlate the applied plastic strain, and thus the dislocation density variation, with changes in hydrogen diffusion coefficient and trap density values. Thin sheets of 42CrMo4_700 were cold rolled to obtain a reduction in thickness of 10% (42CrMo4_700-10%) and 20% (42CrMo4_700-20%). The influence of quenching from a high austenitizing temperature on hydrogen diffusion and trapping was also assessed. For this purpose, 42CrMo4_700 plates were austenitized at 1200ºC for 20 minutes followed by oil quenching and tempering at 700ºC for 2h, obtaining the coarse-grained steel grade denoted as 42CrMo4_700-CG

2.2 Microstructural characterization

The microstructures of the heat-treated steels were examined using a JEOL-JSM5600 scanning electron microscope (SEM), under an acceleration voltage of 20 kV. The samples were previously ground, then polished with diamond paste and finally etched with Nital-2%. Vilella's reagent etching was also used to determine the average prior austenite grain size. Vickers hardness measurements, applying a load of 30 kg for 15 s, were performed on the base and coarser grained steel grades (42CrMo4_700 and 42CrMo4_700-CG) as well as in the deformed (42CrMo4_700-10% and 42CrMo4_700-20%) samples. At least five measurements were made in all cases, subsequently calculating the average hardness value.

2.3 Electrochemical hydrogen permeation tests

The hydrogen transport and trapping behaviour of 42CrMo4 steel quenched and tempered at 700ºC for 2 h (42CrMo4_700, 10% and 20% plastically deformed and coarse-grained steel) was characterized by means of electrochemical permeation tests. Flat specimens measuring 20x20 mm were machined and ground until a thickness of 1.1 mm. Then, both surfaces were ground with 1200 grit SiC paper to achieve a final sample thickness of 1±0.05 mm. A circular exposed area of 1.25 cm^2 was always used.

The permeation tests were performed in a double electrolytic cell based on the one developed by Devanathan and Stachurski [12], as shown in Fig. 1(a). With an approximate volume of 300 ml, both cells satisfy the ASTM G148 [13] recommendation of a solution volume-to-surface area ratio greater than 20 ml/cm^2.

Both cells are separated by the specimen, which is the working electrode (WE) in each cell. The cathodic cell, where hydrogen generation takes places (hydrogen is cathodically generated and adsorbed on the surface of the metal via the application of a cathodic current), was filled with an acid solution (pH≈1) composed of 1M H_2SO_4 and 0.25g/l As_2O_3 to mitigate hydrogen recombination reactions. The other side of the specimen, the anodic cell, where hydrogen oxidation occurs, was filled with a basic solution (pH≈12.5) of 0.1M NaOH. The hydrogen reduction and oxidation reactions that take place in each cell, are shown in Fig. 1(b). Thin platinum plates with a total surface area of 1 cm^2 (similar to the specimen's permeated area) were used as counter electrodes (CE). A reference silver-silver chloride electrode (Ag/AgCl, RE) with a Luggin capillary was employed in the anodic cell and the equipment used for data acquisition was a *pocketSTAT Ivium* potentiostat with a current operation range of ±10 mA. All tests were performed at room temperature.

Before commencing the tests, it is necessary to decrease the background current density in the anodic cell to a steady-state value below 0.1 $\mu A/cm^2$ (which must be subtracted from the measured oxidation current prior to data analysis). To this end, an homogeneous palladium coating (around 1-2 µm thick measured by SEM) was electrodeposited on the anodic side of the sample from a commercial palladium bath containing 2 g/l Pd, applying a current density of 3 mA/cm^2 for 5 min. Hydrogen oxidation is thereby enhanced in the anodic cell, ensuring a virtually zero hydrogen concentration on the exit side of the specimen (Fig. 1(b)). In fact, there is general consensus as to the importance of using palladium coatings on the detection side of ferrous samples so that the permeation results may be reliably exploited, in order to ensure the oxidation of hydrogen atoms on palladium-coated surfaces under most charging conditions [40]. Moreover, the possibility of having introduced hydrogen in the sample during the process of Pd electrodeposition was discarded, as different hydrogen measurements were performed on the Pd-coated samples obtaining values below 0.1 ppm in all cases.

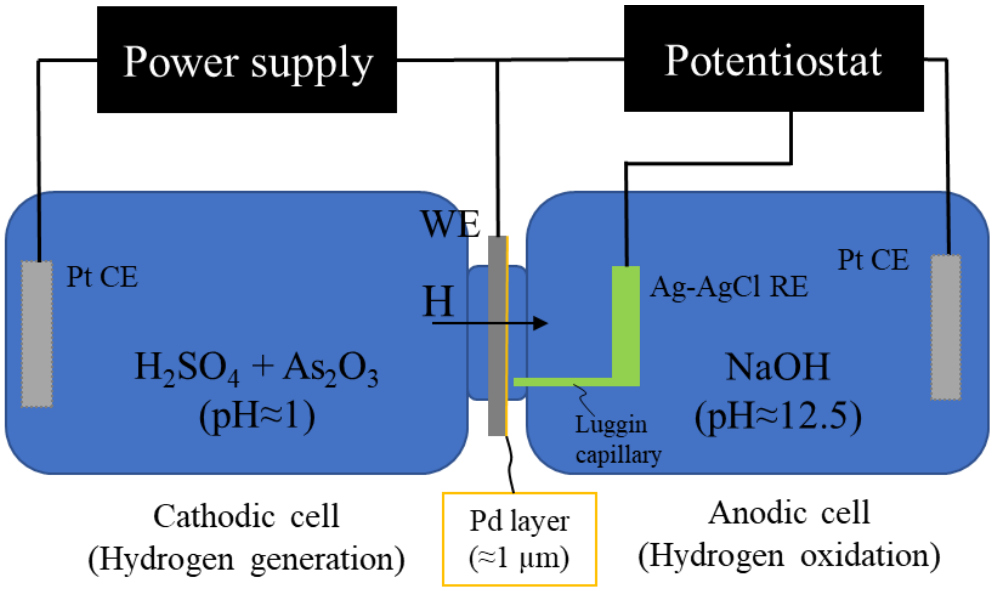

(a)

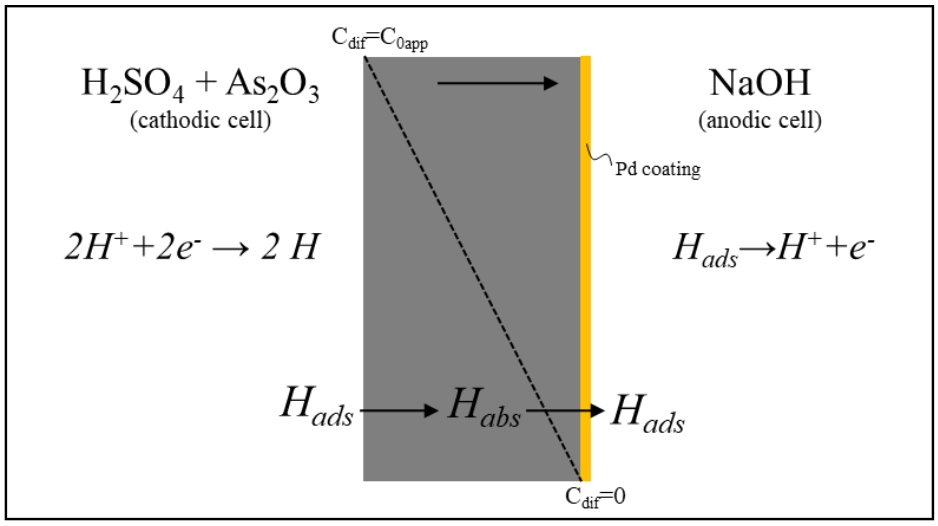

(b)

Fig. 1 (a) Scheme of the modified D-S double-cell employed in the hydrogen permeation experiments; (b) hydrogen reduction and oxidation reactions.

Consequently, the permeation method employed in this study, shown in Fig. 2(a), consisted in record several partial build-up permeation transients by sequentially increasing the cathodic current density until reaching a steady-state value of the hydrogen diffusion coefficient. Operating in this way, saturation of all the microstructural traps is ensured in the last transient, thus allowing the true value of the lattice hydrogen diffusion coefficient of the steel, D_L (hydrogen diffusion barely affected by the presence of microstructural traps) to be obtained. Different stepped permeation tests were performed under different cathodic current densities in order to obtain a complete set of data under cathodic current densities ranging from 0.25 to 4-6 mA/cm^2, depending on the steel grade.

Additionally, single permeation transients, such as the one shown in Fig. 2(b), were also recorded in order to experimentally measure the amount of hydrogen introduced in the specimens once a steady-state hydrogen flux (J_{ss}) was achieved. Single permeation tests were performed under different cathodic current

densities (0.25, 0.5, 0.75, 1 and 2 mA/cm^2) in order to establish the relationship between the cathodic current, hydrogen diffusion coefficient and hydrogen concentration in the steel.

The hydrogen content was measured at the end of the single permeation tests on a LECO DH603 hydrogen analyser. Before starting the measurement, the sample was cleaned with acetone and carefully dried using cold air. The analysis to determine the hydrogen concentration consisted in keeping the sample at 1100ºC for 400 s and is based in the difference in thermal conductivity between a reference gas flow of pure nitrogen and a secondary flow composed of nitrogen and the hydrogen thermally extracted from the sample.

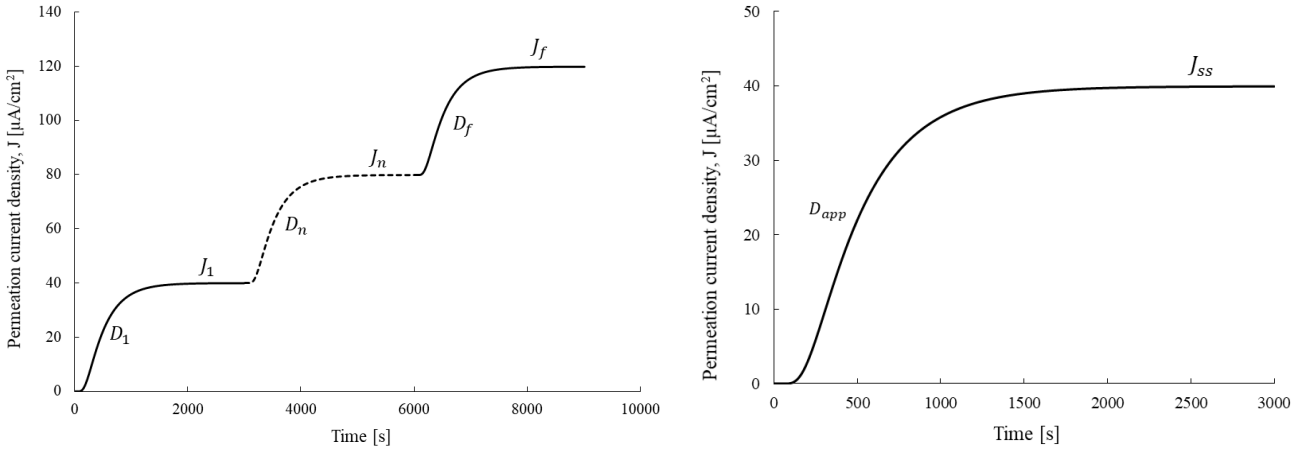

(a) (b)

Fig. 2. Hydrogen permeation build-up tests: (a) stepped permeation transients and (b) single permeation transient

The apparent hydrogen diffusion coefficient, D_{app}, was calculated for each permeation transient according to the "time lag, t_{lag}," method, using Equation (1), derived from Fick's solutions under the appropriate boundary conditions [13].

$$D_{app} = \frac{L^2}{M \cdot t_{lag}} \quad (1)$$

Where *L* is the specimen thickness; t_{lag}, the time needed to reach 63% of the steady-state permeation current, J_{ss}; and *M*, a constant with a value equal to 6 (for $J=63\%J_{ss}$).

The apparent sub-surface hydrogen concentration on the charging side of the sample, C_{0app}, can be determined according to Equation (2):

$$C_{0app} = \frac{J_{ss} \cdot L}{D_{app} \cdot F} \quad (2)$$

where J_{ss} is the steady state permeation current and *F*, the Faraday constant (96485 C/mol). C_{0app} can be converted from mol/cm^3 to ppm wt. by multiplying by M_H/ρ_{Fe}, M_H being the molar mass of hydrogen (1 g/mol) and ρ_{Fe} the density of iron (7.87 g/cm^3).

The relationship between the hydrogen generated by cathodic polarization on the charging side of the specimen, J_c, and the permeation current density detected on the exit side, J_{ss}, obeys Equation (3), in which η is the efficiency of the permeation process, which mainly depends on the hydrogen recombination rate ($H_{ads}+H_{ads} \rightarrow H_2$ (gas)) at the entry surface.

$$J_{ss} = \eta \cdot J_c \quad (3)$$

- *Trap density evaluation*

Stepped build-up hydrogen permeation transients were also used to evaluate the concentration of trapped hydrogen, N_t. The mathematical formulation that allows the calculation of N_t is based on the formalisms developed by McNabb-Foster [41] and Oriani [10], subsequently improved by Kumnick and Johnson [28, 42], who proposed two different approaches for determining the value of N_t depending on the degree of trap occupancy.

When trap occupancy is low, the density trapping sites, N_t, can be determined according to Equation (4),

$$N_t = N_L \left(\frac{D_L}{D_{app}} - 1 \right) \cdot exp\left(-\frac{E_b}{R \cdot T} \right) \quad (4)$$

where D_L is the value of the lattice hydrogen diffusion coefficient of the studied steel (obtained in the last transient, when all traps are filled); D_{app} the apparent hydrogen diffusion coefficient calculated in the first permeation transient to guarantee low trap occupancy; E_b the trap binding energy; R the gas constant and; T, the absolute temperature (298 K). As many authors have considered 27-30 kJ/mol a typical value for hydrogen trapped in dislocations in steels [22, 26, 43-45] and other authors have determined values in the range 24-30 kJ/mol for typical reversible traps in steels [24, 32, 34, 46, 47], an E_b value of 27 kJ/mol was considered in this paper. N_L is the density of the interstitial sites in the steel, which can be calculated as proposed by Krom and Bakker [48], by means of Equation (5).

$$N_L = \frac{N_A \cdot \beta \cdot \rho_{Fe}}{M_{Fe}} \quad (5)$$

N_A being the Avogadro constant (6.022×10^{23} at/mol); β=6, the number of tetrahedral interstitial sites per atom in the Fe BCC crystal lattice; M_{Fe}, the molar mass of iron (55.8 g/mol); and ρ_{Fe}, the density of iron (7.87 g/cm^3). The value of N_L obtained using Equation (5) is 5.1×10^{29} sites/m^3.

For high trap occupancy (trap saturation), the trapping site density, N_t, was calculated following Equation (6):

$$N_t = \frac{C_{0app}}{3} \left(\frac{D_{LFe}}{D_L} - 1 \right) \cdot N_A \quad (6)$$

where C_{0app} is the apparent hydrogen sub-surface concentration in the charging side of the sample, calculated from Equation (2) in the last build-up transient; D_L is the lattice hydrogen diffusion coefficient estimated in this last build-up transient, where traps are fully filled; D_{LFe} is the value of the lattice hydrogen diffusion coefficient in pure iron (a value of 7.3×10^{-9} m^2/s, as reported by [49], was considered in this paper), and N_A is the Avogadro constant. Authors such as [43, 50, 51], among others, used this same approach.

3. RESULTS

3.1 Microstructural characterization

The microstructure of the 42CrMo4 steel austenitized at 845ºC for 45 minutes, quenched in water and tempered at 700ºC for 2h (42CrMo4_700, fine grain) is shown in Fig. 3(a, b). It consists of tempered martensite, with a HV hardness of 207 and an average prior austenite grain size (PAGS) of 20 µm, measured on the as-quenched steel, whose microstructure is shown in Fig. 3(e).

The profuse carbide precipitation that has taken place during the tempering stage can be clearly observed. These carbides (Fe-Cr rich carbides [52, 53]) are evenly distributed throughout the microstructure, with the larger, elongated carbides (with lengths of between 0.5 and 1 μm, Fig. 3(b)) located in the interfaces of the martensitic laths (the average width of this units is around 0.5 μm, and the spherical and smaller carbides (smaller than 0.5 μm) precipitated inside these laths (Fig. 3(b))

The Vickers hardness, HV, measured in the cold rolled samples of 42CrMo4_700 steel was 244 and 259 for plastic deformations of 10% and 20% respectively. The increase in hardness with respect to the base steel is associated with an increase in dislocation density resulting from work hardening.

Fig. 3(c, d) shows the microstructure corresponding to the 42CrMo4 steel grade with a coarser grain size (42CrMo4_700-CG), produced using a higher austenitizing temperature. The microstructure also consists of tempered martensite with homogeneous carbide precipitation. However, this steel grade presents a PAGS of 150 μm (with a corresponding increase in the average size of its martensite laths and packets), which was also measured in the as-quenched condition, Fig. 3(f). This finding can be explained in terms of the greater thermal drop applied to quench the 42CrMo4_700-CG steel grade (quenched from 1200ºC, instead of from 845ºC in the case of 42CrMo4_700). A more distorted martensitic structure is hence produced, with higher internal stresses and, consequently, a higher dislocation density [54], which is reflected in its higher hardness of 230 HV. Distortion differences between these two steel grades can be qualitatively appreciated comparing the morphology of martensite lath and block interfaces (yellow dotted lines in Fig. 3(b, d)).

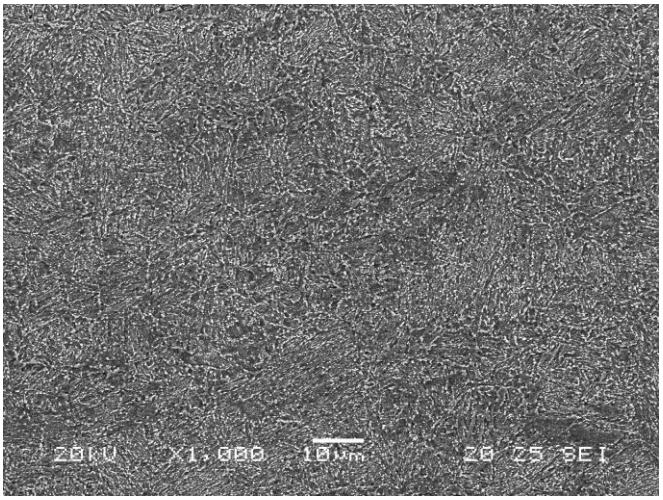

(a)

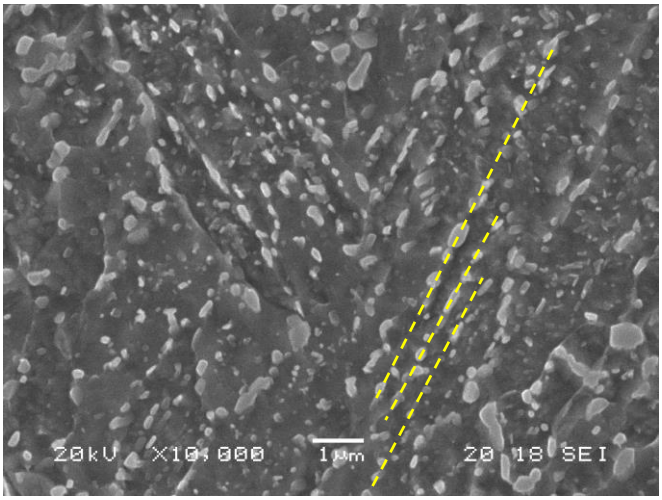

(b)

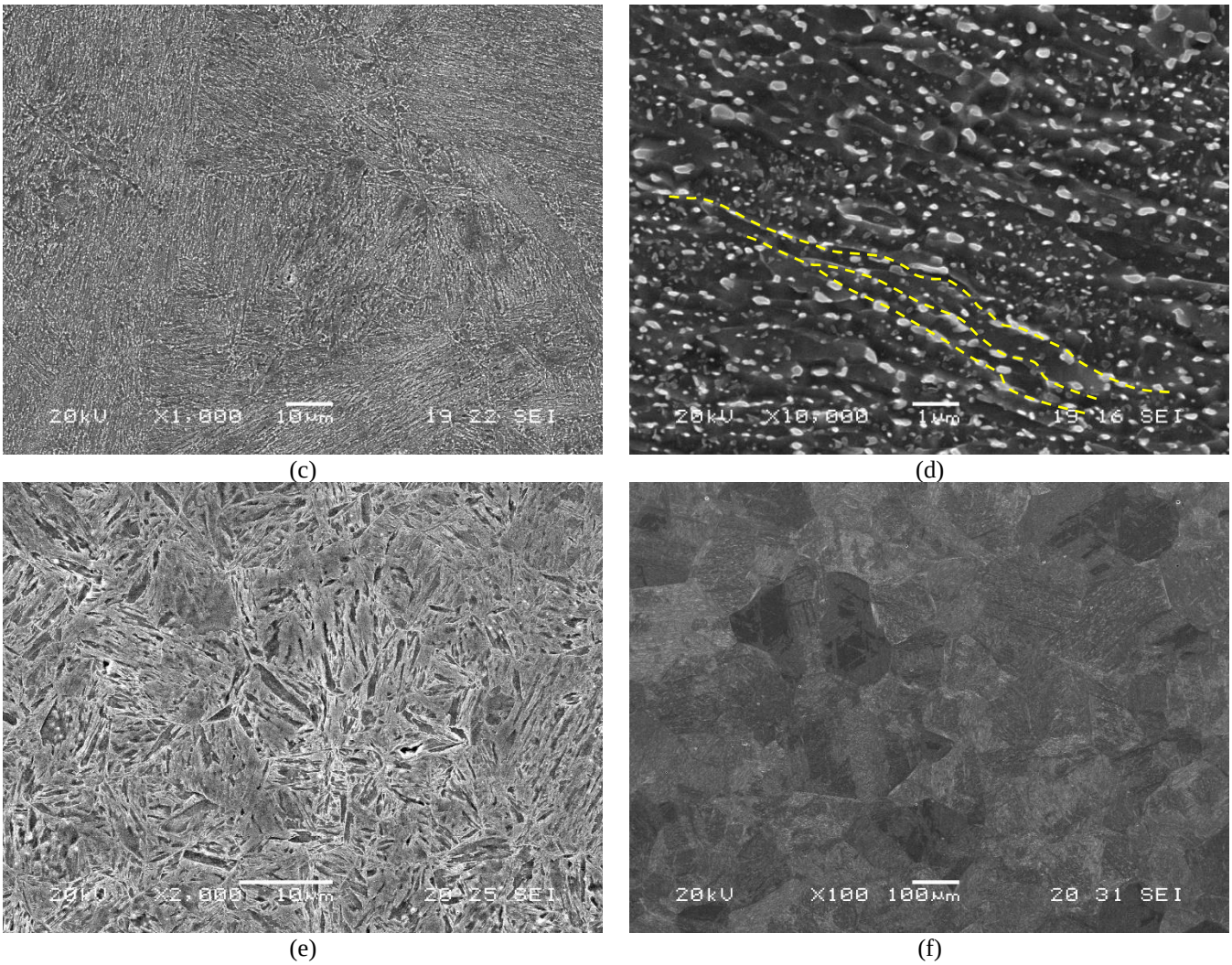

Fig. 3. SEM microstructures of the (a, b) 42CrMo4_700 and (c, d) 42CrMo4_700-CG steel grades (dotted lines show interfaces between martensitic laths). PAGS observed in the as-quenched microstructures of (e) fine-grain and (f) coarse-grain steel grades

3.2 Evolution of the hydrogen diffusion coefficient in 42CrMo4_700

Fig. 4 shows the evolution of the permeation current, J, in the successive permeation build-up transients produced when the cathodic current density in the charging cell, J_c, was incrementally increased from 0.5 mA/cm^2 up to a final current density of 4 mA/cm^2 using 0.5 mA/cm^2 steps. Table 3 gives the values of the applied cathodic current density, J_c, and the steady-state permeation current density, J_{ss}, along with the efficiency of the process, η. The apparent hydrogen diffusion coefficient obtained using the time lag value (Equation (1)) in each transient, D_{app}, and the apparent hydrogen sub-surface cathodic concentration, C_{0app} (Equation (2)), are also included in the same table.

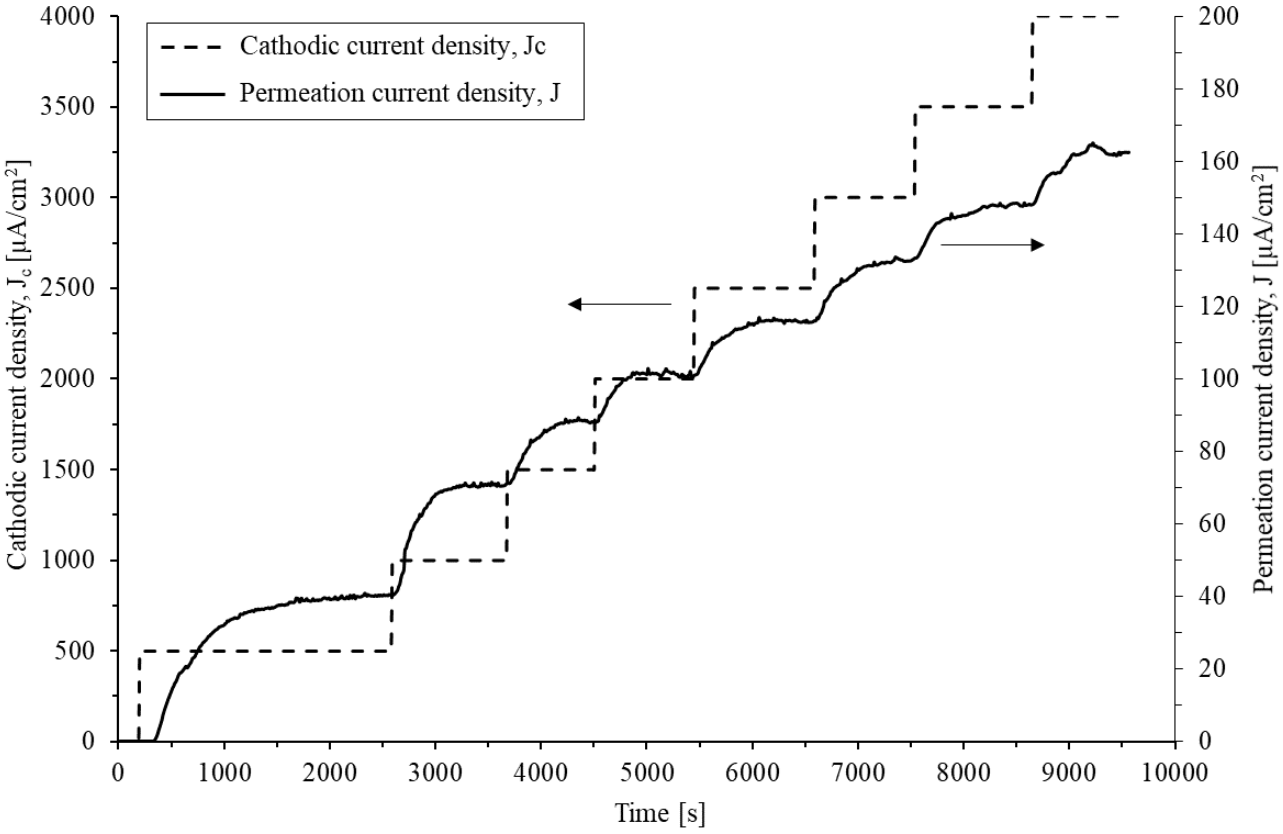

Fig.4. Evolution of the permeation current density, J, for successive increments of the cathodic current density, J_c. 42CrMo4_700. Applied J_c: 0.5+0.5+0.5+0.5+0.5+0.5+0.5+0.5 mA/cm²

Table 3. Values of the cathodic current density, J_c; steady-state permeation current density, J_{ss}; efficiency of the permeation process, η; time lag, t_{lag}; apparent hydrogen diffusion coefficient of each permeation transient, D_{app}; and apparent subsurface hydrogen concentration on the charging side of the specimen, C_{0app}

Permeation transient	J_c [mA/cm²]	J_{ss} [µA/cm²]	η [%]	t_{lag} [s]	D_{app} [m²/s]	C_{0app} [ppm]
1	0.5	40.3	7.8	555	2.7×10^{-10}	--
2	1.0	70.4	6.8	215	7.0×10^{-10}	1.26
3	1.5	88.6	5.7	220	6.8×10^{-10}	1.62
4	2.0	100.8	4.8	180	8.4×10^{-10}	1.51
5	2.5	116.2	4.5	225	6.7×10^{-10}	2.17
6	3.0	132.6	4.3	260	5.8×10^{-10}	2.87
7	3.5	148.0	4.1	190	7.9×10^{-10}	2.34
8	4.0	161.8	3.9	230	6.5×10^{-10}	3.10

Note that an increase in the cathodic current density is always followed by a proportional jump in the steady-state permeation current, reflecting an increase in the subsurface hydrogen concentration on the charging side of the specimen. A fairly uniform D_{app} value was already obtained after the second step.

The relationship between J_c and J_{ss} is the efficiency of the permeation process, Equation (3), which depends mainly on the hydrogen fugacity in the cathodic face of the specimen. Fig. 5 provides a graphic representation of the value of η versus the applied cathodic current density. Note that the efficiency of the process is considerably low (below 8%) and continuously decreases with increasing the applied cathodic current density. This information is useful to establish cathodic charging conditions, where the use of low charging current densities (between 0.5-2 mA/cm²) is more convenient.

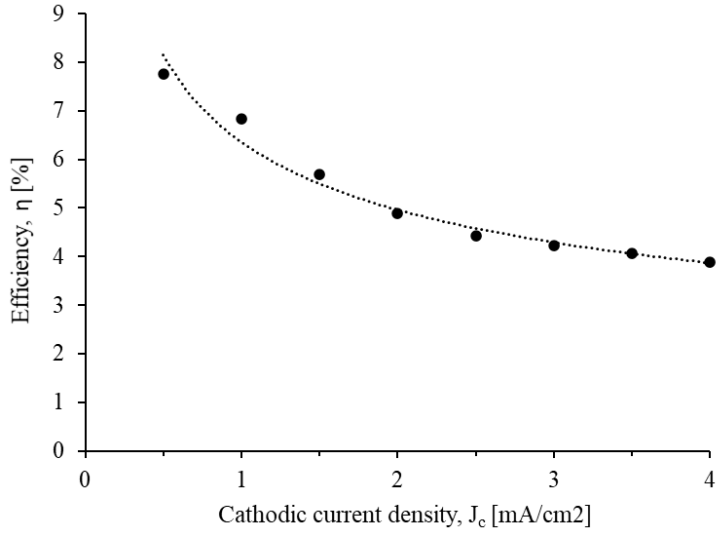

Fig. 5. Efficiency, η, of the permeation process vs. the applied cathodic current density, J_c. 42CrMo4_700. Applied J_c: 0.5+0.5+0.5+0.5+0.5+0.5+0.5+0.5 mA/cm^2

The results of all the stepped permeation tests carried out under different cathodic current densities with the 42CrMo4_700 steel grade are shown in Fig. 6, in which the evolution of the apparent hydrogen diffusion coefficient is represented versus the applied cathodic current density. In accordance with the work carried out by Raina et al. [16], three different regimes can be distinguished depending on trap occupancy:

(I) In the first build-up transient, the hydrogen traps are empty, and the obtained apparent diffusion coefficient is the lowest. An average value of 2.7×10^{-10} m^2/s was measured under applied J_c values of 0.25 and 0.5 mA/cm^2, corresponding to hydrogen transport under high interaction of hydrogen atoms with microstructural traps.

(II) Hydrogen atoms progressively fill the microstructural traps present in the steel, the effect of traps progressively decreases and, consequently, the D_{app} value increases in this region.

(III) Finally, the hydrogen traps become practically saturated and there is no more trapping effect, only lattice diffusion. Thus, the hydrogen diffusion coefficient becomes approximately constant, regardless of the applied cathodic current density. This value corresponds to the lattice hydrogen diffusion coefficient of the steel, D_L. An average D_L value of around 8×10^{-10} m^2/s was obtained with the results corresponding to the highest J_c density currents.

It is thus evident that the stepped build-up transient method employed in this study is suitable for studying hydrogen diffusion evolution with microstructural hydrogen trapping in steels, ultimately allowing the determination of the so-called lattice hydrogen diffusion coefficient, D_L.

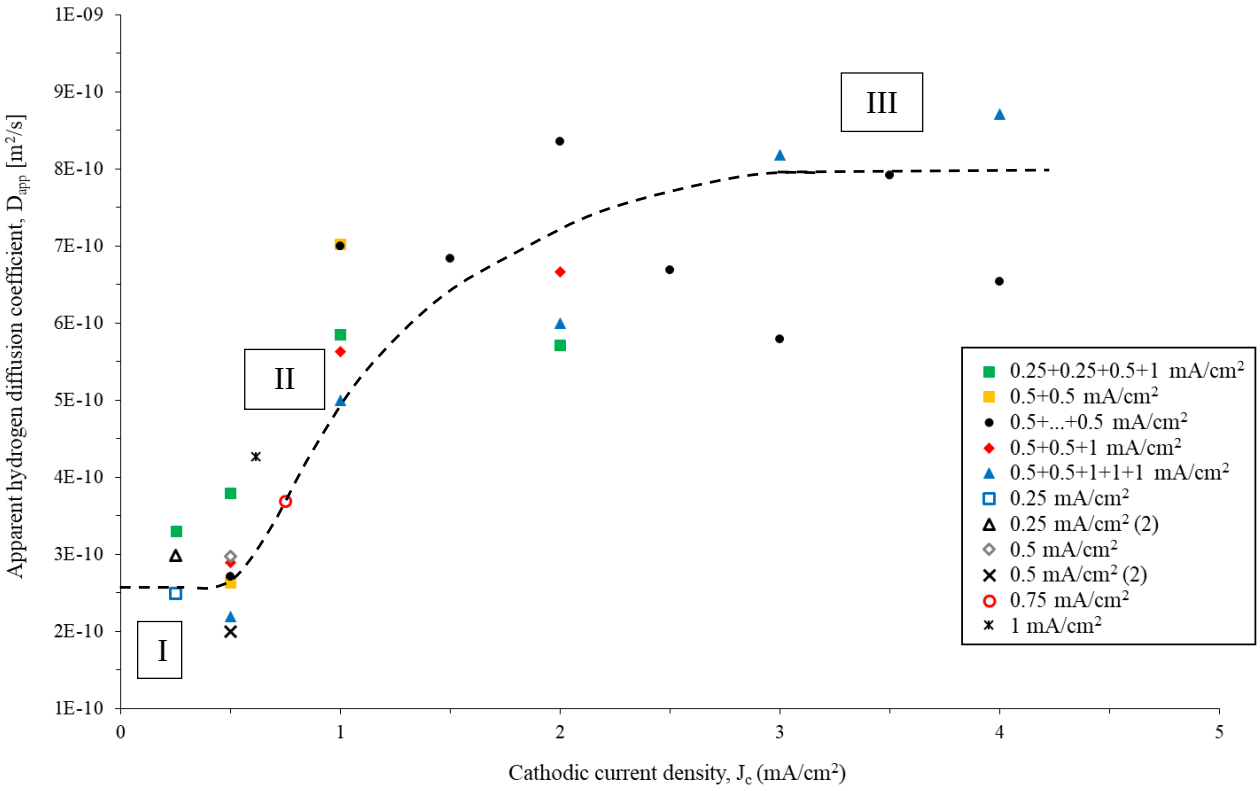

Fig. 6. The apparent hydrogen diffusion coefficient, D_{app}, vs. the applied cathodic current density, J_c obtained in all the build-up permeation transients. 42CrMo4_700.

3.3 Determination of hydrogen contents in 42CrMo4_700

Experimental hydrogen measurements were performed in the Leco DH 603 hydrogen analyser after cathodic charging in order to correlate the evolution of the apparent hydrogen diffusion coefficient not only with the applied cathodic current density, but also with the total hydrogen concentration introduced in the steel microstructure, C_T. With this aim in mind, single permeation transients were recorded under 0.25, 0.5, 0.75, 1 and 2 mA/cm^2 cathodic current densities, using 1 mm thickness samples of 42CrMo4_700 grade.

In order to obtain an accurate value of the hydrogen concentration in the permeated specimen at the end of the single permeation tests, a simple unidirectional diffusion finite element analysis (FEA) was performed using Abaqus, employing Fick´s law described in Equation (7), in order to correct the permeated area, where hydrogen is trapped. J represents the hydrogen flux; D_{app} the apparent hydrogen diffusion coefficient; and C_H, the hydrogen concentration in the specimen.

$$J = -D_{app}\,\nabla C_H \qquad (7)$$

A caption of the hydrogen distribution during the course of a permeation process through a 1 mm-thick steel membrane is presented in Fig. 7. A hydrogen permeation area of 1.33 cm^2 was determined when the initial permeation area on the charging side of the specimen was 1.25 cm^2. A correction factor of 1.06 was subsequently employed to calculate C_T in Table 4.

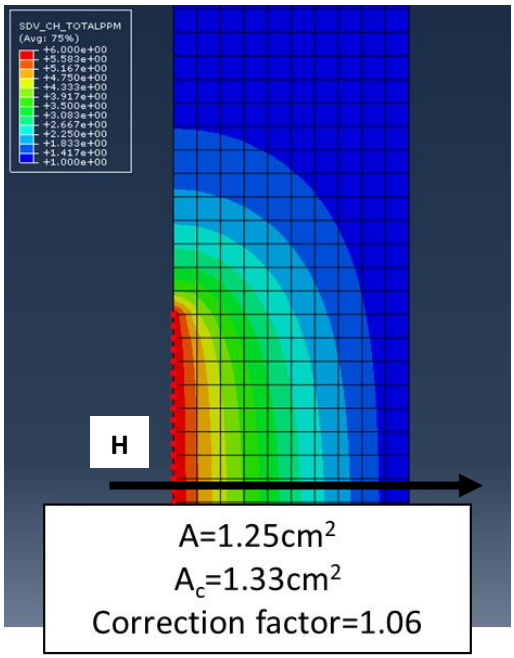

Fig.7. Abaqus simulation. Hydrogen distribution during the course of a permeation experiment using a membrane thickness of 1 mm

The values of the experimentally determined total hydrogen concentrations, C_T, are shown in Table 4, along with the corresponding values of the steady-state permeation density currents, J_{ss}.

Table 4. Hydrogen concentration determined using a Leco analyser, C_T, after hydrogen charging under different cathodic current densities in single permeation tests

J_c [mA/cm^2]	J_{ss} [µA/cm^2]	C_T [ppm]
0.25	21.8	0.78
0.5	40.8	1.03
0.75	49.2	2.32
1	77.4	4.16
2	105.8	4.15

Finally, Fig. 8 shows the relationship obtained between the apparent diffusion coefficient, D_{app} and the experimentally measured total hydrogen concentration in the specimen, C_T. The three zones already shown in Fig. 6 were now also defined as a function of the total hydrogen concentration present in the steel. The lattice hydrogen diffusion coefficient of the steel, D_L, was reached when the total hydrogen concentration in the steel was between 3 and 4 ppm (most of the microstructural hydrogen traps were filled).

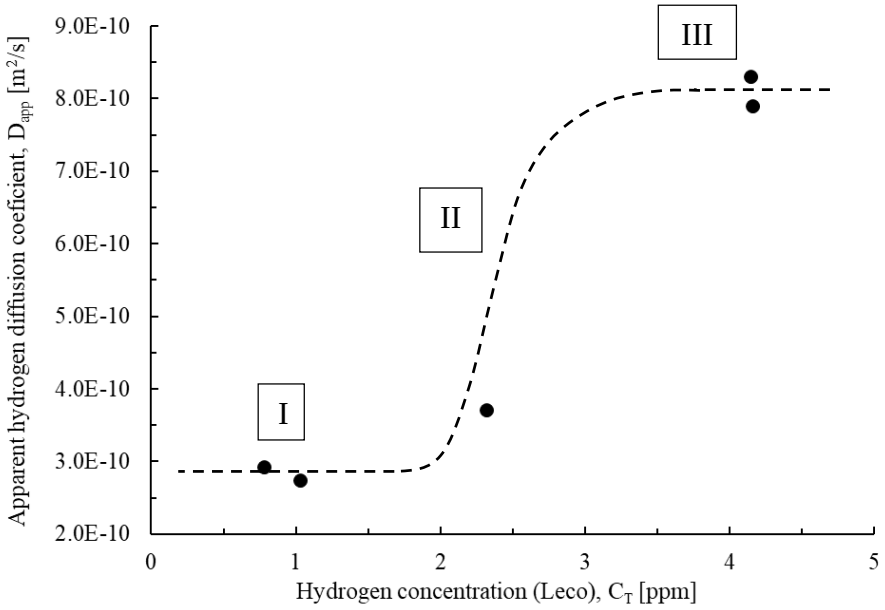

Fig.8. Apparent hydrogen diffusion coefficient vs. average hydrogen concentration in the specimen, C_T

3.4 Influence of quenching from a high austenitizing temperature

In order to compare the behaviour of the 42CrMo4_700 and 42CrMo4_700-CG steel grades, the permeation curves corresponding to the stepped build-up transients (0.5→4 mA/cm^2) obtained under cathodic current density increments of 0.5+0.5+1+1+1 mA/cm^2 are shown in Fig. 9. Table 5 provides the values, for both steel grades, of the applied cathodic current density, J_c, the steady-state permeation current density, J_{ss}, the apparent hydrogen diffusion coefficient obtained in each transient, D_{app}, and the apparent hydrogen sub-surface cathodic concentration calculated on the charging side of the specimen, C_{0app} (these values can only be calculated when D_{app} reaches a stable value; the last transient in these cases).

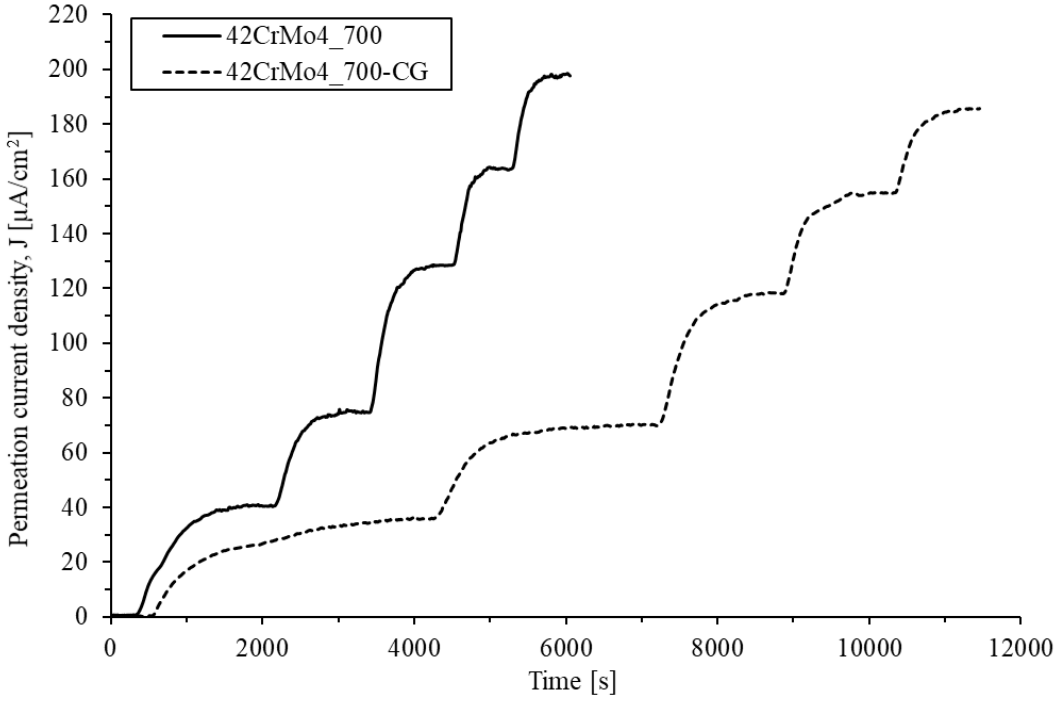

Fig. 9. Stepped permeation transients of base and coarse-grained 42CrM4-700 steel. Applied J_c: 0.5+0.5+1+1+1 mA/cm^2

Table 5. Influence of prior austenite grain size on stepped permeation transients under applied J_c values of 0.5+0.5+1+1+1 mA/cm^2. Current density, J_c; steady-state permeation current density, J_{ss}; apparent hydrogen diffusion coefficient of each permeation transient, D_{app}, and apparent subsurface hydrogen concentration on the charging side of the specimen, C_{0app}

Permeation transient	J_c [mA/cm^2]	42CrMo4_700			42CrMo4_700-CG		
		J_{ss} [μA/cm^2]	D_{app} [m^2/s]	C_{0app} [ppm]	J_{ss} [μA/cm^2]	D_{app} [m^2/s]	C_{0app} [ppm]
1	0.5	40.4	2.2×10^{-10}	---	35.7	1.5×10^{-10}	---
2	1	74.0	5.0×10^{-10}	---	70.1	3.6×10^{-10}	---
3	2	127.2	6.0×10^{-10}	---	118.3	4.9×10^{-10}	---
4	3	161.1	8.2×10^{-10}	2.33	154.8	6.6×10^{-10}	---
5	4	194.7	8.7×10^{-10}	2.65	185.6	7.4×10^{-10}	3.51

Note that the measured value of D_{app} is lower in the coarser grain microstructure for all the applied cathodic current densities, while the C_{0app} values are higher. Quenching the steel from a higher austenitizing temperature yields a coarser, more distorted martensitic structure, with higher internal stresses and hence a higher dislocation density. These differences are maintained after the final tempering treatment, thereby explaining the aforementioned results. In line with our results, [36] also measured a lower hydrogen diffusion coefficient, along with higher dislocation density and structural distortion, as quenching temperature is increased (larger austenite grain size) in a Cr-Mo-V steel quenched and tempered at 700ºC. On the other hand, the first and successive D_{app} values obtained with the base 42CrMo4_700 steel barely differ from those already presented in Table 3.

Fig. 10, which (similarly to Fig. 6) shows the evolution of the apparent hydrogen diffusion coefficient in terms of the applied cathodic current density, gathers all the data obtained with all the permeation tests performed on the coarse-grained steel grade, 42CrMo4_700-CG, using different cathodic current densities. The average lowest value of the apparent diffusion coefficient, determined in the first build-up transient when hydrogen diffuses through a microstructure with empty traps, is around 2.2×10^{-10} m^2/s, while the lattice hydrogen diffusion coefficient of this steel, D_L, is around 7×10^{-10} m^2/s.

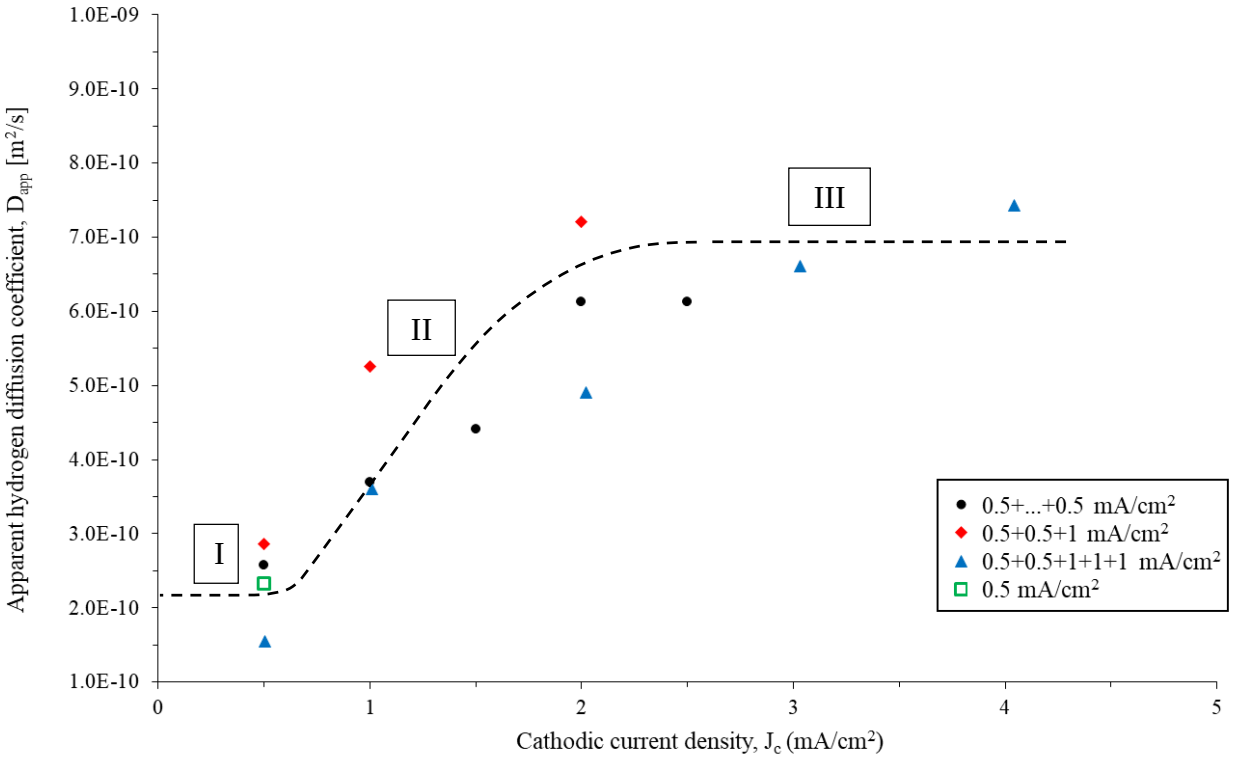

Fig. 10. Evolution of the apparent hydrogen diffusion coefficient, Dapp, vs. the applied cathodic current density, J_c. Coarse grain 42CrMo4_700-CG

Moreover, Table 6 now presents the trap occupancy or density of trapping sites, N_t, determined on the two steel grades using Equations (4) and (6). An increase in the density of trapping sites in the coarse-grained steel grade was obtained. Furthermore, given that an approximate and hypothetical single trap binding energy (E_b=27 kJ/mol) was employed in Equation (4), the density of hydrogen trapping sites obtained using both equations was quite similar (in both steel grades). The average value of N_t is also presented in Table 6. It is also noted that most carbides are aligned along martensite lath interfaces (Fig. 3), where dislocations also concentrate, being difficult to separate and differentiate tempered carbides, martensite lath, block and packet interfaces and dislocations as hydrogen traps in quenched and tempered steels. The E_b value we have used in the manuscript is usually assigned to dislocations but, as we have already mentioned, carbides and internal interfaces co-exist with dislocations on the same location.

Table 6. Influence of the prior austenitic grain size on the density of trapping sites, N_t, calculated for low and high trap occupancy levels

PAGS [μm]	N_t [sites/m^3]		
	Equation (4)	Equation (6)	Average
20	2.56×10^{25}	1.45×10^{25}	2.01×10^{25}
150	3.61×10^{25}	2.42×10^{25}	3.02×10^{25}

3.5 Influence of plastic deformation

The successive transients obtained from the permeation tests performed on the 42CrMo4_700 steel grade with plastic deformations of 0%, 10% and 20% are shown in Fig. 11, while the corresponding values of D_{app} and C_{0app} are given in Table 7. Note that D_{app} does not reach a stable value until the final transients and C_{0app} can only be calculated in those last build-up transients. Additionally, Fig. 12 shows, as in the previous cases, the evolution of the apparent hydrogen diffusion coefficient in terms of the applied cathodic current density.

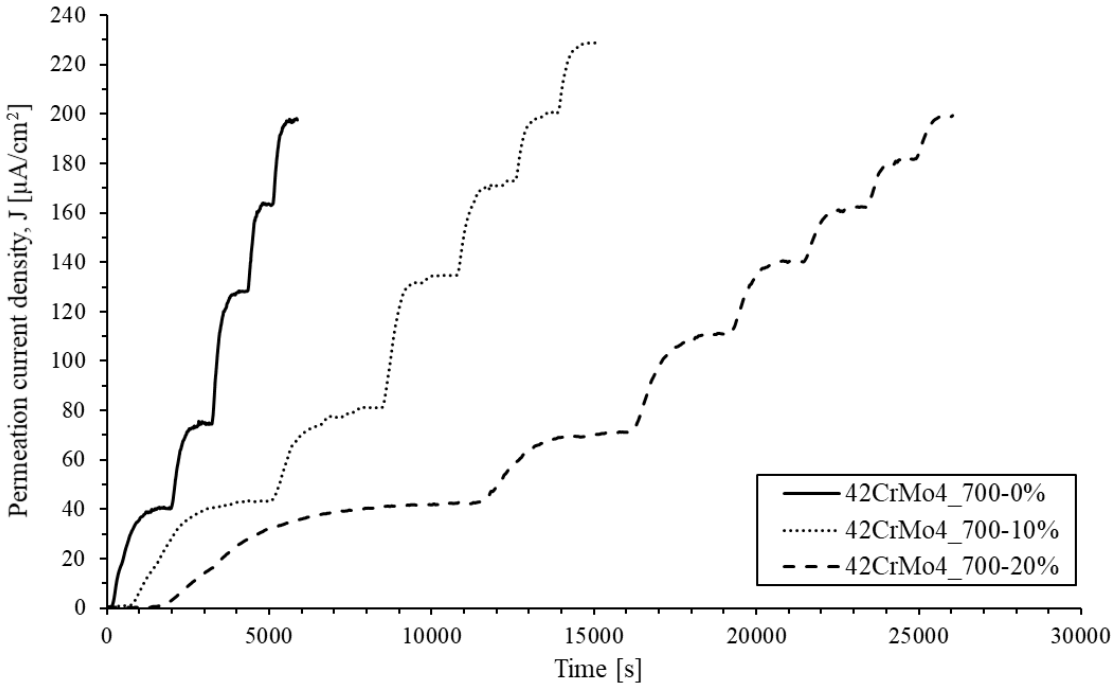

Fig. 11. Stepped permeation transients for 42CrMo4: plastic deformations of 0%, 10% and 20%. Applied J_c: 0.5+0.5+1+1+1 mA/cm²

Table 7. Influence of plastic deformation in stepped permeation transients. Test: 0.5+0.5+1+1+1+1+1 mA/cm². Current density, J_c; steady-state permeation current density, apparent diffusion coefficient of each permeation transient, D_{app}; and apparent subsurface hydrogen concentration on the charging side of the specimen, C_{0app}

Permeation transient	J_c [mA/cm²]	ε_p=0%		ε_p=10%		ε_p=20%	
		D_{app} [m²/s]	C_{0app} [ppm]	D_{app} [m²/s]	C_{0app} [ppm]	D_{app} [m²/s]	C_{0app} [ppm]
1	0.5	2.2×10^{-10}	---	5.6×10^{-11}	---	2.8×10^{-11}	---
2	1	5.0×10^{-10}	---	1.4×10^{-10}	---	8.2×10^{-11}	---
3	2	6.0×10^{-10}	---	2.3×10^{-10}	---	1.3×10^{-10}	---
4	3	8.2×10^{-10}	2.33	3.1×10^{-10}	---	1.8×10^{-10}	---
5	4	8.7×10^{-10}	2.65	4.3×10^{-10}	5.00	2.4×10^{-10}	---
6	5	---	---	4.3×10^{-10}	5.72	3.0×10^{-10}	6.66
7	6	---	---	---	---	3.3×10^{-10}	6.74

The apparent hydrogen diffusion coefficient, D_{app}, measured under all the cathodic current densities decreases with increasing plastic deformation, due to the increase of the dislocation density, which hinders diffusion of hydrogen through the steel microstructure. Plastic deformation provides a cellular dislocation distribution, in which dislocation in cell walls increase and cell size decreases with the applied deformation [20, 31, 55]. This effect is quite evident for the first transient in which hydrogen atoms fill the microstructural traps present in the steel, where a decrease of nearly an order of magnitude was observed in D_{app} between the base steel and the 20% plastically deformed steel. Moreover, the measured lattice hydrogen diffusion coefficient when most of the traps are filled, D_L, respectively decreases from a value of 8.7×10^{-10} m²/s for the base steel to 4.3×10^{-10} m²/s and 3.2×10^{-10} m²/s when the steel is plastically deformed 10 and 20%.

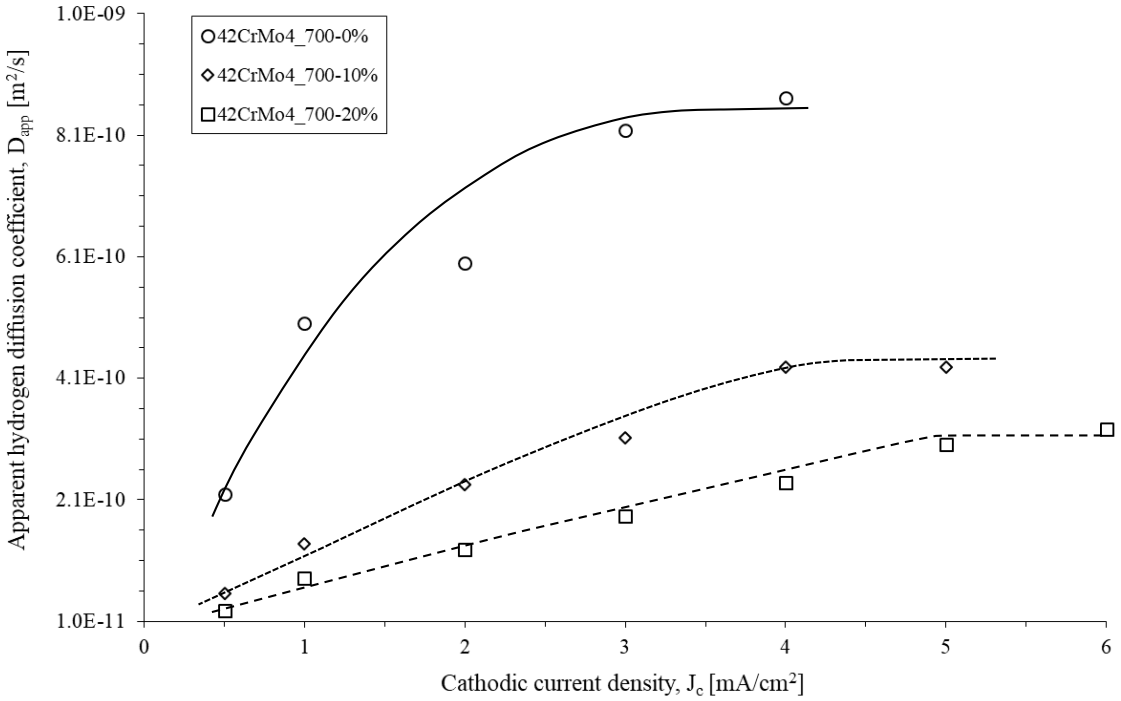

Fig. 12. Evolution of the apparent hydrogen diffusion coefficient, D_{app}, vs. the applied cathodic current density, J_c. 42CrMo4_700 with plastic deformation of 0, 10 and 20%

Similarly to the evolution of D_{app} and D_L, the apparent subsurface hydrogen concentration on the charging side of the specimen, C_{0app}, and trap density, N_t, also increases with plastic deformation, as can be seen in Table 8, due to the increase in structural defects, mainly dislocations, which act as reversible hydrogen traps. The values of N_t obtained using Equations (4) and (6) also present quite similar results except in the case of the 20% plastically deformed steel, in which a something higher value was calculated using Equation (6). Nonetheless, it should be recalled here than an approximate single trap binding energy, E_b, of 27 kJ/mol was employed in Equation (4) and the result obtained using this equation is highly dependent on the selected E_b value. Average N_t values are also presented in Table 8.

Table 8. Influence of plastic deformation on the reversible trap density, N_t, calculated for low and high trap occupancy levels

Plastic deformation [%]	C_{0app} [ppm]	N_t [sites/m^3]		
		Equation (4)	Equation (6)	Average
0	2.33	2.56×10^{25}	1.45×10^{25}	2.01×10^{25}
10	5.00	6.27×10^{25}	6.26×10^{25}	6.27×10^{25}
20	6.74	1.00×10^{26}	1.13×10^{26}	1.06×10^{26}

Fig. 13 shows the relationship between the steel hardness, HV, the value of the apparent hydrogen diffusion coefficient, D_{app}, for low trap occupancy (first permeation transient using 0.5 mA/cm^2), the lattice hydrogen diffusion coefficient, D_L, when the microstructural traps are saturated with hydrogen (last permeation transient) and the value of the apparent sub-surface hydrogen concentration on the charging side of the specimen, C_{0app}, when the specimen has reached saturation (last transient). Note the good correlation obtained between the aforementioned permeation properties and the hardness of the different steel grades, as this basic mechanical property provides an indirect measure of the dislocation density, which is the structural parameter that governs hydrogen diffusion and trapping in martensitic steels.

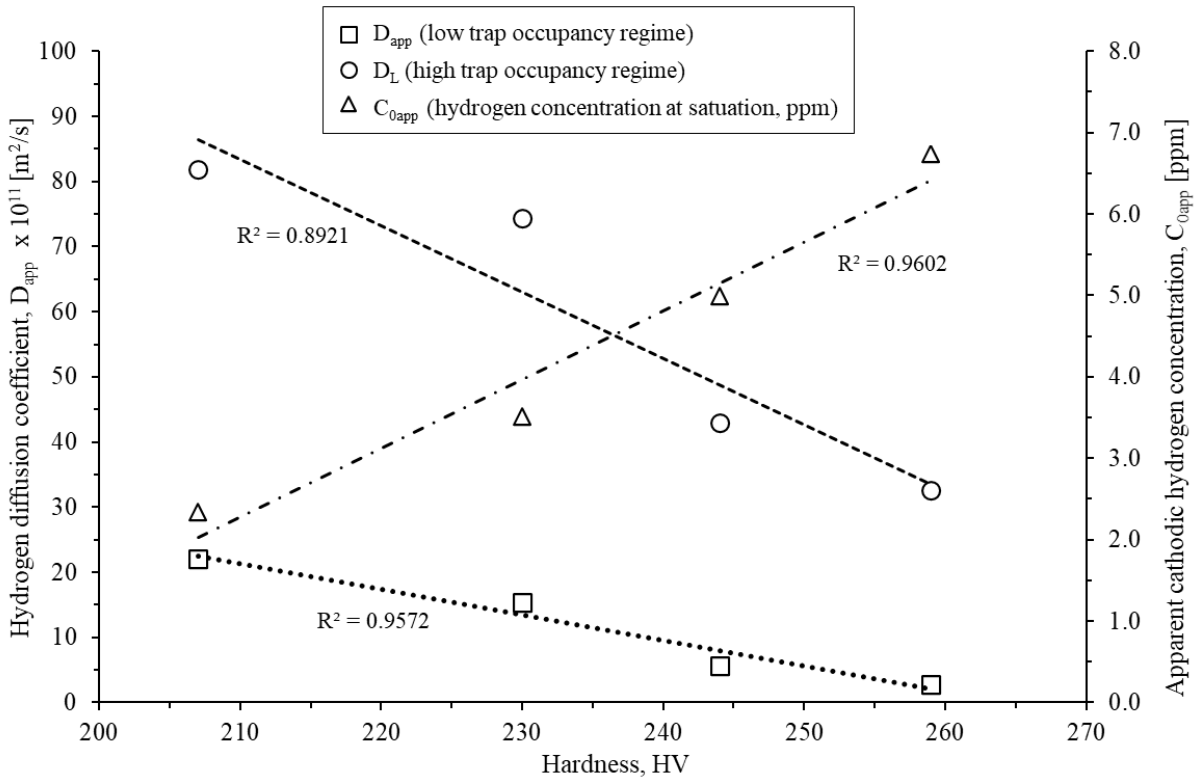

Fig. 13. Relationship between the hardness HV, lattice and apparent hydrogen diffusion coefficients, D_L, D_{app} and apparent cathodic hydrogen concentration, C_{0app}

Additionally, Fig. 14(a) shows the relationship between the true plastic strain, ε_p, and the average density of hydrogen trap sites, N_t. The results showed in this figure are in line with those obtained by other authors. Works reported in [56,57] are based on permeation tests, while [58] obtained their results assuming one trap per atomic plane threaded by a dislocation. It is also known that different steels have different trap densities based on their specific microstructures, as can be appreciated when the initial value at ε_p=0 is compared (data from [56] are based in a refined iron, while [57] used a carbon steel).

On the other side, Fig. 14(b) shows a good linear fitting between the density of trapping sites and steel hardness, because hydrogen trapping in quenched and tempered steels is mainly due to dislocations, as it was already mentioned.

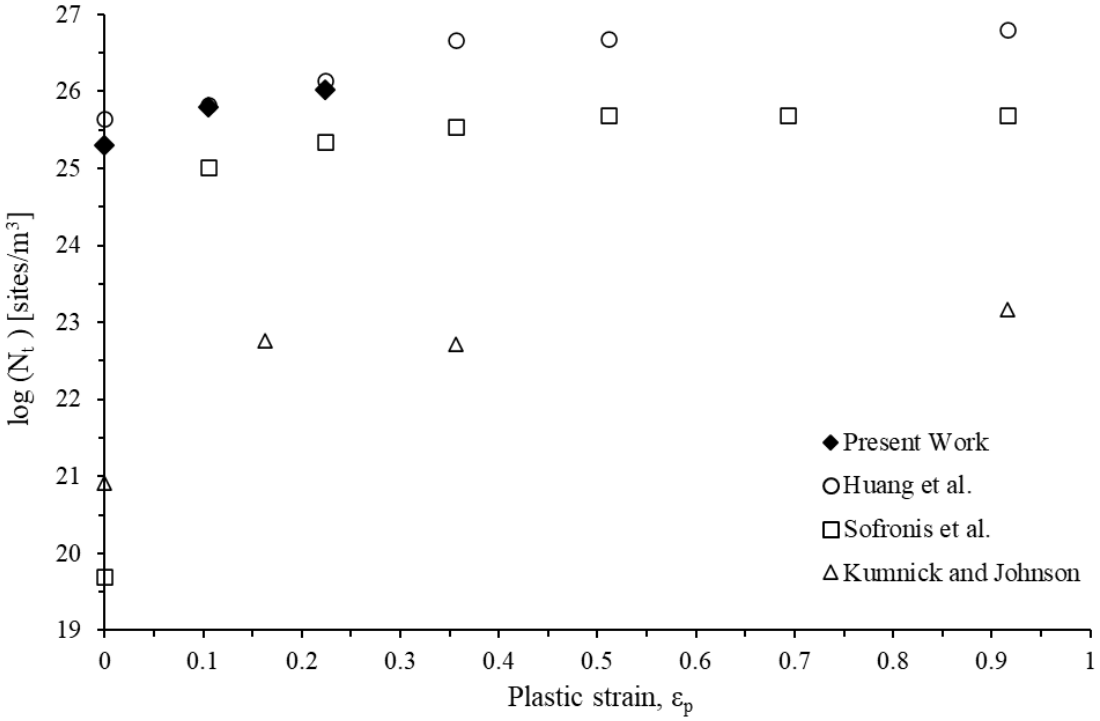

(a)

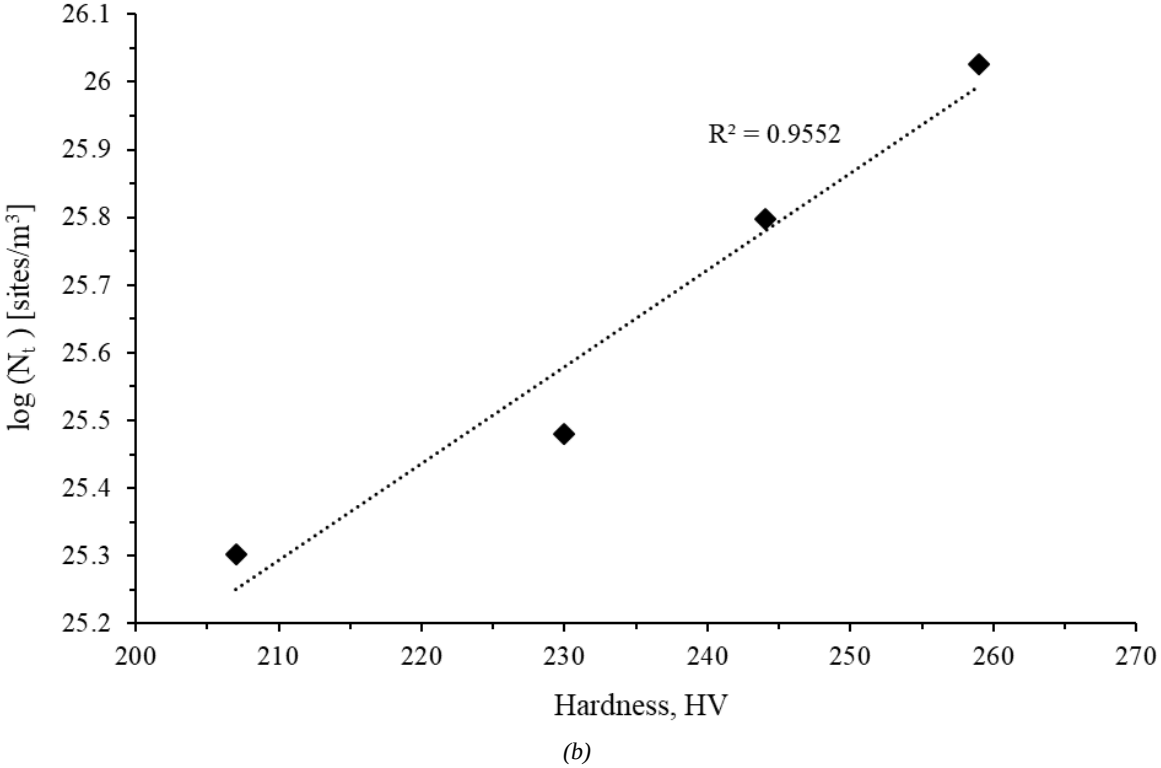

(b)

Fig. 14. (a) Trap density, N_t, versus plastic strain, ε_p. Results from Kumnick and Johnson [56], Huang et al. [57] and Sofronis et al. [58] are also included in the figure; (b) Relationship between hardness HV and the average reversible trap density, Nt (linear regression)

4. CONCLUSIONS

The microstructure of a 42CrMo4 steel which was quenched after austenitized at 845ºC for 40 min and tempered at 700°C for 2 h consisted of tempered martensite (PAGS of 20 μm and a hardness of 207 HV), characterized by martensitic laths and packets and profuse precipitation of Fe,Cr-rich carbides. Plastic deformations of 10% and 20% were applied, increasing the hardness of the steel up to 244 HV and 259 HV, respectively. Furthermore, quenching the steel from a higher austenitizing temperature (1200ºC instead of 845ºC) gave rise to a coarser and more distorted martensitic structure, with a PAGS of around 150 μm and a hardness of 230 HV, with higher internal stresses and hence higher dislocation density.

Due to trapping phenomenon, a single value for the hydrogen diffusion coefficient, D, is not representative of permeation performance. In this case, the relationship between trap occupancy and the apparent diffusion coefficient, D_{app}, was determined by means of stepped build-up transients. In the first transient, when the hydrogen traps are empty, the D_{app} coefficient reaches a minimum value, increasing as the traps are progressively filled, until saturation is completed and the lattice hydrogen diffusion coefficient, D_L, of the steel is reached.

The apparent hydrogen diffusion coefficient, D_{app}, decreases and trapping density increases with increasing plastic deformation, due to the multiplication of dislocation density, which hinders diffusion of hydrogen through the steel microstructure. On the other hand, the coarse-grain microstructure produced via quenching the steel from a higher austenitizing temperature has lower D_{app} values than the base fine grain steel and higher density of hydrogen traps.

A good linear correlation was obtained between the permeation properties (diffusion coefficients, hydrogen absorption capability and density of hydrogen trap sites) and the hardness of the different steel grades, as this basic mechanical property provides an indirect measure of the dislocation density in martensitic microstructures, which is the structural parameter that governs hydrogen diffusion and trapping in steels.

AKNOWLEDGEMENTS

The authors would like to thank the Spanish Ministry of Science, Innovation and Universities for the financial support received to carry out research project RTI2018-096070-B-C31 (H2steelweld). A. Zafra is grateful to the Ministry of Education and Culture of the Principality of Asturias for the Severo Ochoa grant (PA-18-PF-BP17-038). Authors also thank the financial support received from the Principado de Asturias government through the FC-GRUPIN-IDI/2018/000134 project.

DATA AVAILABILITY

The raw/processed data required to reproduce these findings cannot be shared at this time as the data also forms part of an ongoing study.

REFERENCES

[1] C.D. Kim, Hydrogen-damage failures, in Metals Handbook, vol. 11, Failure Analysis and Prevention, American Society for Metals, Metals Park, Ohio, USA, 1986.

[2] A.L. Marcelo, R. C. Tokimatsu, I. Ferrera, Hydrogen embrittlement in an AISI 1045 steel component of the sugarcane industry, Eng. Fail. Anal. 16 (2009) 468-474.

[3] G. Straffelini, L. Versari, Brittle intergranular fracture of a thread: The role of a carburizing treatment, Eng. Fail. Anal. 16 (2009) 1448-1453.

[4] M. Yan, Y. Weng, Study on hydrogen absorption of pipeline steel under cathodic charging, Corros. Sci. 48 (2006) 432-444.

[5] S. Takagi, Y. Toji, M. Yoshino, K. Hasegawa, Hydrogen embrittlement resistance evaluation of ultra-high strength steel for automobiles, ISIJ Int. 52-2 (2012) 316-322.

[6] A. Oudriss, A. Fleurentin, G. Courlit, E. Conforto, C. Berziou, C. Rebere, S. Cohendoz, J.M. Sobrino, J. Creus, X. Feugas, Consequences of the diffusive hydrogen contents on tensile properties of martensitic steel during desorption at room temperature, Mat. Sci. Eng. A 598 (2014) 420-428.

[7] Y. Murakami, T. Kanezaki, P. Sofronis, Hydrogen embrittlement of high strength steels: Determination of the threshold stress intensity for small cracks nucleating in non-metallic inclusions, Eng. Fract. Mech. 97 (2013) 227-243.

[8] C. Colombo, G. Fumagalli, F. Bolzoni, G. Gobbi, L. Vergani, Fatigue behaviour of hydrogen pre-charged low alloy Cr-Mo steel, Int. J. Fatigue 83 (2016) 2-9.

[9] H. Bhadeshia. Prevention of hydrogen embrittlement in steels. ISIJ Int. 56-1 (2016) 24-36.

[10] R.A. Oriani, The diffusion and trapping of hydrogen on steels, Acta Metall. 18 (1970) 147-157.

[11] H. J. Grabke, E. Riecke, Absorption and diffusion of hydrogen in steels, Mater. Technol. 34 (2000) 331-342.

[12] M.A.V. Devanathan, Z. Stachurski, The adsorption and diffusion of electrolytic hydrogen in palladium, P. R. Soc. A270 (1962) 90-102.

[13] ASTM G148, Standard practice for evaluation of hydrogen uptake, permeation, and transport in metals by an electrochemical technique, ASTM International, PA, United States, 2011.

[14] T. Zakroczymski, Adaptation of the electrochemical permeation technique for studying entry, transport and trapping of hydrogen in metals, Electrochim. Acta 51 (2006) 2261-2266.

[15] T. Zakroczymski, Z. Szklarska-Smialowska, Activation of the Iron surface to hydrogen absorption resulting from a long cathodic treatment in NaOH Solution, J. Electrochem. Soc. 132 (1985) 2548.

[16] A. Raina, V.S. Deshpande, N.A. Fleck, Analysis of electro-permeation of hydrogen in metallic alloys, Phil. Trans. R. Soc. A375: 20160409 (2017) 1-16.

[17] S. Frappart, X. Feaugas, J. Creus, F. Thebault, L. Delattre, H. Marchebois, Study of the hydrogen diffusion and segregation into Fe-C-Mo martensitic HSLA Steel using electrochemical permeation test, J. Phys. Chem. Solids 71 (2010) 1467-1479.

[18] A. Turnbull, Perspectives on hydrogen uptake, diffusion and trapping, Int. J. Hydrogen Energy 40 (2015) 16961-16970.

[19] T. Schaffner, A. Hartmaier, V. Kokotin, M. Pohl, Analysis of hydrogen diffusion and trapping in ultra-high strength steel grades, J. Alloy. Compd. 746 (2018) 557-566.

[20] C. Park, N. Kang, M. Kim, S. Liu, Effect of prestrain on hydrogen diffusion and trapping in structural steel, Mater. Lett. 235 (2019) 193-196.

[21] Q. Liu, J. Venezuela, M. Zhang, Q. Zhou, A. Atrens, Hydrogen trapping in some advanced high strength steels, Corr. Sci. 111 (2016) 770-785.

[22] Q. Liu, A. Atrens, Reversible hydrogen trapping in a 3.5NiCrMoV medium strength steel, Corr. Sci. 96 (2015) 112-120

[23] T. Zakroczymski, Electrochemical determination of hydrogen in metals, J. Electroanal. Chem. 475 (1999) 82-88.

[24] E. Fallahmohammadi, F. Bolzoni, L. Lazzari, Measurement of lattice and apparent diffusion coefficient of hydrogen in X65 and F22 pipeline steels, Int. J. Hydrogen Energy 38 (2013) 2531-2543.

[25] E. Fallahmohammadi, F. Bolzoni, G. Fumagalli, G. Re, G. Benassi, L. Lazzari, Hydrogen diffusion into three metallurgical microstructures of a C-Mn X65 and low alloy F22 sour service Steel pipelines, Int. J. Hydrogen Energy 39 (2014) 13300-13313.

[26] P. Zhou, W. Li, H. Zhao, X. Jin, Role of microstructure on electrochemical hydrogen permeation properties in advanced high strength steels, Int. J. Hydrogen Energy 43 (2018) 10905-10914.

[27] D. Rudomilova, T. Prosek, P. Salvetr, A. Knaislová, P. Novák, R. Kodým, G. Schimo-Aichhorn, A. Muhr, H. Duchaczek, G. Luckeneder, The effect of microstructure on hydrogen permeability of high strength steels, Mater. Corros. (2019) 1-9.

[28] A. Kumnick, H. Johnson, Hydrogen transport through annealed and deformed Armco iron, Metall. Trans. 5 (1974) 1199-1206.

[29] K. Kiuchi, R. McLellan, The solubility and diffusivity of hydrogen in well-annealed and deformed iron, Acta Metall. 31 (1983) 961-984.

[30] P. Castaño-Rivera, N. de Vincentis, R. Bolmaro et al., Relationship between dislocation density and hydrogen trapping in a cold worked API 5L X60 steel, P. Mater. Sci. 8 (2015) 1031-1038.

[31] Y.D. Han, R.Z. Wang, H. Wang, L.Y. Xu, Hydrogen embrittlement sensitivity of X100 pipeline steel under different pre-strain, Int. J. Hydrogen Energy 44 (2019) 22380-22393.

[32] R. Gibala and A. J. Kumnick, Hydrogen trapping in iron and steels, Hydrogen Embrittlement and Stress Corrosion Cracking, ASM, Ohio, USA (1984) 61-77.

[33] I. Maroef et al., Hydrogen trapping in ferritic steel weld metal, Int. Mater. Rev. 47-4 (2012) 191-223.

[34] J.Y.Lee and J.L. Lee, A trapping theory of hydrogen in pure iron, Philos. Mag. A 57-3 (1987) 293-309.

[35] L. Jemblie, V. Olden, O.M. Akselsen, A couple diffusion and cohesive zone modelling approach for numerically assessing hydrogen embrittlement of steel structures, Phil. Trans. R. Soc. A375: 20160411 (2017) 1-16.

[36] Q. Wang, Y. Sun, S. Gu, Z. He, Q. Wang, F. Zhang, Effect of quenching temperature on sulphide stress cracking behaviour of martensitic steel, Mat. Sci. Eng. A 724 (2018) 131-141.

[37] Y. D. Han, H.Y. Jing, L.Y. Xu, Welding heat input effect on the hydrogen permeation in the X80 steel welded joints, Mater. Chem. Phys. 132 (2012) 216-222.

[38] A. Zafra, L.B. Peral, J. Belzunce, C. Rodríguez, Effect of hydrogen on the tensile properties of 42CrMo4 steel quenched and tempered at different temperatures, Int. J. Hydrogen Energy 43 (2018) 9068-9082.

[39] A.Zafra, L.B. Peral, J. Belzunce, C. Rodríguez, Effects of hydrogen on the fracture toughness of 42CrMo4 steel quenched and tempered at different temperatures, Int. J. Pres.Ves. Pip. 171 (2019) 34-50.

[40] P. Manolatos, M. Jerome, J. Galland, Necessity of a palladium coating to ensure hydrogen oxidation during electrochemical permeation measurements on iron, Electrochim. Acta 40-7 (1995) 867-871.

[41] A. McNabb, P. Foster, A new analysis of the diffusion of hydrogen in iron and ferritic steels, Trans. AIME 227 (1963) 618.

[42] A. J. Kumnick and H.H. Johnson, Deep trapping states for hydrogen, Acta. Metall. 28 (1980) 33-39.

[43] C.F Dong, Z.Y Liu, X.G Li, Y.F Cheng, Effects of hydrogen charging on the susceptibility of X100 pipeline steel to hydrogen induced cracking, Int. J. Hydrogen Energy 34 (2009) 9879-89.

[44] A.J. Haq, K. Muzaka, D.P. Dunne, A. Calka, E.V. Pereloma, Effect of microstructure and composition on hydrogen permeation in X70 pipeline steels, Int. J. Hydrogen Energy 38 (2013) 2544–2556.

[45] A. Begic Hadzipasic, J. Malina, M. Malina, The influence of microstructure on hydrogen diffusion and embrittlement of multiphase fine-grained steels with increased plasticity and strength, Chem. Biochem. Eng. Q. 25 (2011) 159–169.

[46] W.Y. Choo, J. Lee, Thermal analysis of trapped hydrogen in pure iron, Metall. Trans. A 13 (1982) 135-140

[47] M. Enamoto, D. Hirakami, T. Tarui, Modeling thermal desorption analysis of hydrogen in steel, ISIJ Int. 46 (2006) 1381.

[48] A.H.M Krom, A.D. Bakker, Hydrogen trapping models in steel, Metall. Mat. Trans. B. 31 (2000) 1475-1482.

[49] K. Kiuchi, R.B. McLellan, The solubility and diffusivity of hydrogen in well-annealed and deformed iron, Acta Metall. 31 (1983) 961-984.

[50] S.K. Yen, I.B. Huang, Critical hydrogen concentration for hydrogen induced blistering on AISI 430 stainless steel, Mater. Chem. Phys. 80 (2003) 662-666.

[51] H. Izadi, M. Tavakoli, M. H. Moayed, Effect of thermomechanical processing on hydrogen permeation in API X70 pipeline Steel, Mater. Chem. Phys. 220 (2018) 360-365.

[52] N. Parvathavarthini, S. Saroja, R.K. Dayal, H.S. Khatak, Studies on hydrogen permeability of 2.25%Cr1%Mo ferritic steel: correlation with microstructure, J. Nucl. Mater. 288 (2001) 187-196.

[53] Y.F. Jiang, B. Zhang, Y. Zhou, J.Q. Wang, E.H. Han, W. Ke, Atom probe tomographic observation of hydrogen trapping at carbide/ferrite interfaces for a high strength steel, J. Mater. Sci. Technol. 34 (2018) 1344-1348.

[54] George Krauss, Steels: Processing, Structure and Performance. 2005.

[55] B. C. de Cooman, J. G. Speer, Fundamentals of Steel Product Physical Metallurgy, Association for Iron & Steel Technology, Warrendale, PA, USA, 2011.

[56] A.J. Kumnick and H.H. Johnson, Deep trapping states for hydrogen in deformed iron, Acta Metall. 28 (1980) 33-39.

[57] H. Huang, W.J.D. Shaw, Hydrogen embrittlement interactions in cold-worked steel, Corr. Sci. (1995) 30-36.

[58] P. Sofronis, Y. Liang, N. Aravas, Hydrogen induced shear localization of the plastic flow in metals and alloys, Eur. J. Mech. A/Solids. 20 (2001) 857–872.